ISSN 1063-7737, Astronomy Letters, 2015, Vol. 41, No. 12, pp. 765–784. © Pleiades Publishing, Inc., 2015.
Original Russian Text © S.A. Grebenev, I.A. Mereminskiy, 2015, published in Pis'ma v Astronomicheskiĭ Zhurnal, 2015, Vol. 41, No. 12, pp. 826–846.

JEM-X/INTEGRAL X-ray Survey of the Galactic Center Region

S. A. Grebenev* **and I. A. Mereminskiy****

Space Research Institute, Russian Academy of Sciences, Profsoyuznaya ul. 84/32, Moscow, 117997 Russia

Received December 8, 2014

Abstract—An X-ray survey of the Galactic center region with a radius of ∼20° has been performed using the data obtained with the JEM-X telescope onboard the INTEGRAL observatory over ∼10 years of observations (2003–2013). The exposure at the field center directly toward the Galactic center has reached 4.8 Ms. We have constructed sky maps in the 5–10 and 10–25 keV energy bands and compiled a catalog of detected sources. Together with 83 sources revealed on the integral sky maps, it includes 22 transients that are absent on them but are confidently detected during outbursts with a duration of several days. One of the persistent sources, IGR J17452-2909, has never been observed previously. In contrast to the catalog of sources detected in the harder energy band by the IBIS/ISGRI telescope onboard the INTEGRAL observatory, most of the sources in this catalog are low-mass X-ray binaries (73 of the 105 sources) and only 18 + 3 are high-mass X-ray binaries and cataclysmic variables. Out of the Galactic sources, there are also the black hole candidate XTE J1652-453, the peculiar X-ray burster XMM J174457-2850.3, and the soft gamma repeater SGR 1806–20 in the catalog; out of the extragalactic sources, there are three active galactic nuclei and a galaxy cluster (Oph CL). The nature of four sources, including the newly discovered one, still remains unknown. We have constructed the luminosity function for the low-mass X-ray binaries from the catalog and considered other statistical properties of their sample.

DOI: 10.1134/S1063773715120038

Keywords: *X-ray sources, transients, luminosity function.*

INTRODUCTION

The INTEGRAL orbital astrophysical gamma-ray observatory (Winkler et al. 2003) has been monitoring X-ray sources in the Galactic plane and Galactic center field since 2003. Over this period, the observatory has discovered ∼100 previously unknown X-ray binaries in the Galaxy, more than 150 X-ray active galactic nuclei and quasars, and several objects of a different nature. In fact, the number of hard X-ray sources known on the sky has been doubled. The catalogs of detected sources have been published based on the results of observations with the main instrument of the observatory, the IBIS gamma-ray telescope (Ubertini et al. 2003) with the ISGRI array of semiconductor CdTe detectors sensitive in the 20–200 keV band (Lebrun et al. 2003); their updated versions are regularly released (e.g., Revnivtsev et al. 2004b; Molkov et al. 2004; Bird et al. 2010; Krivonos et al. 2010, 2012, 2014; Grebenev et al. 2013).

In this paper, we present the results of an equally deep (ten years of observations) survey of the Galactic center field ∼20° in radius with another INTEGRAL telescope, the *Joint European X-ray Monitor* (JEM-X) (Lund et al. 2003) sensitive in the standard 3–35 keV X-ray band. This is a coded-aperture telescope; its field of view with a diameter of 13.°2 FWZR (the diameter of the fully coded region is 4.°8) is bounded by a collimator. The detector is a gas chamber with an entrance window area of ∼490 cm^2 and an energy resolution $\Delta E/E \sim 16\%$ FWHM at 6 keV. The effective area at the center of the field of view is only ≃75 cm^2, because more than 80% of the detector is shadowed by the opaque mask and collimator elements. There are two identical modules of the telescope onboard the observatory; if they operate simultaneously, then the effective area turns out to be twice as large, ≃150 cm^2. The angular resolution of the JEM-X telescope is a factor of ∼3 higher than that of the IBIS telescope (∼3.′35 FWHM), and, hence, it has an obvious advantage in investigating crowded sky fields (such as the Galactic center and bulge). On the other hand, since the JEM-X field of view is a factor of ∼4 smaller than the IBIS one (29° × 29° FWZR), the total exposure of the regions under study turned out to be appreciably shorter than the IBIS exposure, although both instruments operated almost simultaneously. This naturally limited the

*E-mail: sergei@hea.iki.rssi.ru
**E-mail: i.a.mereminskiy@gmail.com

possibilities of the JEM-X telescope in investigating faint sources.

Note that attempts to summarize the results of individual observations performed with the JEM-X telescope have already been made previously. For example, Westergaard (2009) published the catalog of sources detected by the telescope over the first ∼5 years of observations (from February 2003 to September 2008). The catalog is markedly inferior to our survey in time base, limiting sensitivity, data selection and analysis technique, and number of sources detected in the Galactic center region. Westergaard did not analyze the distribution of sources from the catalog in luminosity and position on the sky. Sanchez-Fernandez (2012) presented a catalog of X-ray bursts detected by JEM-X from bursters. As a rule, these events are much shorter than the time scale of the transient events considered here.

The JEM-X X-ray survey of the Galactic center region may be considered as supplementary to the harder X-ray survey performed with the IBIS/ISGRI telescope. We have demonstrated the efficiency of this approach previously when investigated the Large Magellanic Cloud field (Grebenev et al. 2013). At the same time, we cannot but note that virtually no surveys of such a large (more than 1200 sq. deg.!) area at a sufficiently high (∼1 mCrab) sensitivity and a good (arcmin) angular resolution in the standard X-ray band have been conducted. We can mention the surveys of the Galactic center field by the XRT telescope onboard the SPACELAB-2 station (Skinner et al. 1987), the TTM telescope onboard the MIR–KVANT module (in't Zand et al. 1989; Sunyaev et al. 1991a), and the ART-P telescope onboard the GRANAT observatory (Sunyaev et al. 1991b; Pavlinsky et al. 1994). They all had a small ($\lesssim$100 sq. deg.) area and were performed with a fairly short exposure, i.e., were, as it were, "snapshots" of the sky. The ASCA (Sugizaki et al. 2001; Sakano et al. 2002) and XMM (Warwick et al. 2012) surveys of the central Galactic regions had an even smaller area. The ROSAT all-sky survey (Voges et al. 1999) was performed in a softer ($\leq$2 keV) X-ray band, while the RXTE sky surveys (with the ASM and PCA instruments; Grimm et al. 2002; Revnivtsev et al. 2004a), along with the earlier HEAO 1 sky survey (the A1 experiment; Wood et al. 1984), were conducted with a poor ($\gtrsim 1^\circ$) angular resolution. Therefore, our survey, not to mention the JEM-X all-sky survey being prepared for publication (Meremiskiy and Grebenev 2015), is of great importance in its own right.

SELECTION AND DATA REDUCTION

Because of limitations on the INTEGRAL satellite orientation relative to the solar direction, the Galactic center region was accessible to observation twice a year, in early spring and fall, each time approximately for two months. To perform the survey and compile the catalog of detected sources, we used all publicly available data of the telescope from February 2003 to April 2013 (revolutions 40–1237). We selected individual pointings of the observatory in directions offset by less than 26° from the Galactic center with an exposure time of more than 500 s (typically, the exposure is 1.5–3.5 ks). The shorter exposures were rejected to reduce the systematic noise. After the selection, ∼25 000 individual pointings with a total duration of ≈61 Ms remained. The exposure of the central zone near the Galactic center with a radius of ∼2° reached 4.8 Ms; the median exposure in the Galactic plane was ≈1 Ms. To analyze the sources and to construct the sky images, we used only the central region 20° in radius with an exposure everywhere above 10 ks (Fig. 1). The effective (with an optimal sensitivity) 5–25 keV energy band of the telescope was divided into two subbands: soft 5–10 keV and hard 10–25 keV; the entire analysis was performed for these subbands separately and independently.

Since the JEM-X telescope is equipped with a coded aperture, a special computer analysis of the input data is required to reconstruct the sky images. To obtain the images in individual pointings, we used the OSA 10.0 software developed at the INTEGRAL Science Data Center of the University of Geneva.[1] The images obtained were analyzed and then added using the software specially developed for this task at the Space Research Institute of the Russian Academy of Sciences. In our analysis, we searched for sources in the images in several steps. Initially, all bright known sources whose flux exceeded the detection threshold were found in the image. Subsequently, they were successively removed (subtracted) from the image, whereupon the distribution of 3-by-3 pixel cells (roughly corresponding to the point spread function) in total significance was constructed. The cells that stood out statistically ($\geq 3.5\sigma$) compared to the Gaussian distribution were checked for the presence of a source by taking into account the local background. To determine the background, we used 40-by-40-pixel regions around the selected cells; the detection limit was set at the 5σ level. This approach allowed even fairly faint sources in noisy fields to be confidently detected.

After the analysis of individual images, we constructed composite maps (mosaics) from individual revolutions (three days in duration) and integral mosaics from all observations in the two chosen energy bands. The JEM-X telescope consists of two similar,

[1] http://www.isdc.unige.ch/integral/analysis

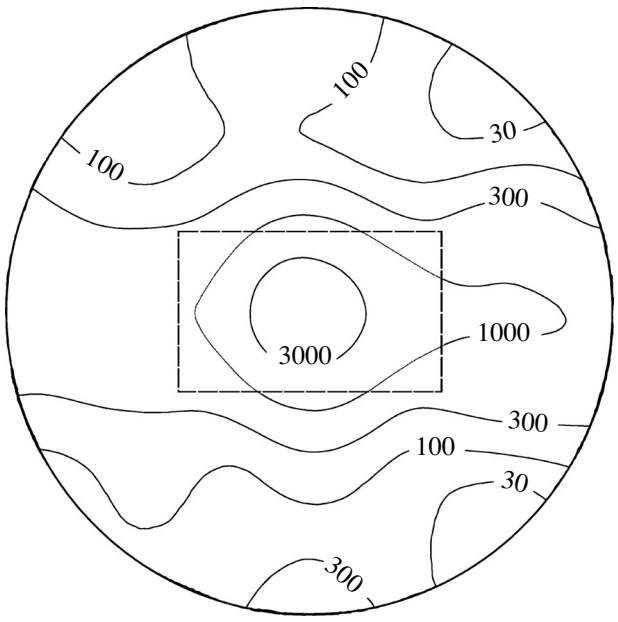

Fig. 1. Distribution of exposures for the JEM-X observations of the Galactic center region in 2003–2013. The contours correspond to exposures of 30, 100, 300, 1000, and 3000 ks. In the region with a radius of ∼20° indicated by the circumference, the exposure nowhere drops below 10 ks. The dashed line bounds the rectangular region for which Fig. 2 presents the integral sky images.

though not quite identical modules (Lund et al. 2003). At different stages of the mission, the observations were carried out either simultaneously by the two modules or separately by one or the other module. For our analysis, the data from both modules were used in a unified way, despite a slight difference in collecting area (≈0.5 and ≈2% for the soft and hard channels, respectively).

In constructing the mosaics to increase the signal-to-noise ratio, we excluded the regions at the edge of the JEM-X field of view in which the noise was great due to weaker illumination by the emission from sources suppressed by the collimator; only the central region of the images with a radius of 5.°7 was used. The search for sources on the integral mosaics and the mosaics from individual revolutions was carried out similarly to their search in the individual images.

The data from all available observations of the Crab Nebula were added to calibrate the measured fluxes from sources. As a result, we found that a flux of 1 Crab gives 0.065 and 0.036 counts s^{-1} cm^{-2} in the 5–10 and 10–25 keV energy bands, respectively. Note that the flux of 1 mCrab in these energy bands is 9.0×10^{-12} and 1.05×10^{-11} erg s^{-1} cm^{-2}, respectively.

RESULTS

The individual sky images obtained allow the variability of detected sources to be investigated on various time scales. In this paper, we restrict ourselves to presenting only the integral sky maps and the catalog of sources detected on them and discuss in detail the statistical properties and spatial distribution of the separate populations of sources. We touch the questions of variability only in connection with the detection of transients, leaving its detailed discussion for a separate paper.

S/N Maps

Figure 2 shows the integral (obtained over the entire time of INTEGRAL observations of this field) S/N maps for the central 18° × 11° Galactic center region in the two chosen energy bands. This region is indicated in Fig. 1 by the dashed line. To improve perception of the figure the maps were convolved with a Gaussian of 3′ in radius. Positions of 32 known quasi-persistent X-ray sources shown on the maps by yellow circles and that of the Galactic nucleus—by a green circle. It can be seen that some of the sources, for example, XTE J1739-285, SLX 1746-331, SLX 1746-370, and GRS 1747-312, are brighter in the soft X-ray image, while others, such as GRS 1734-292, GRS 1758-258, and GX 3+1, are brighter in the hard one. Of course, this is indicative of differences in spectral hardness of these sources.

Because of inaccuracies in the available model of the telescope mask, it is virtually impossible to completely take into account the detector response to a specific source. There are many bright sources

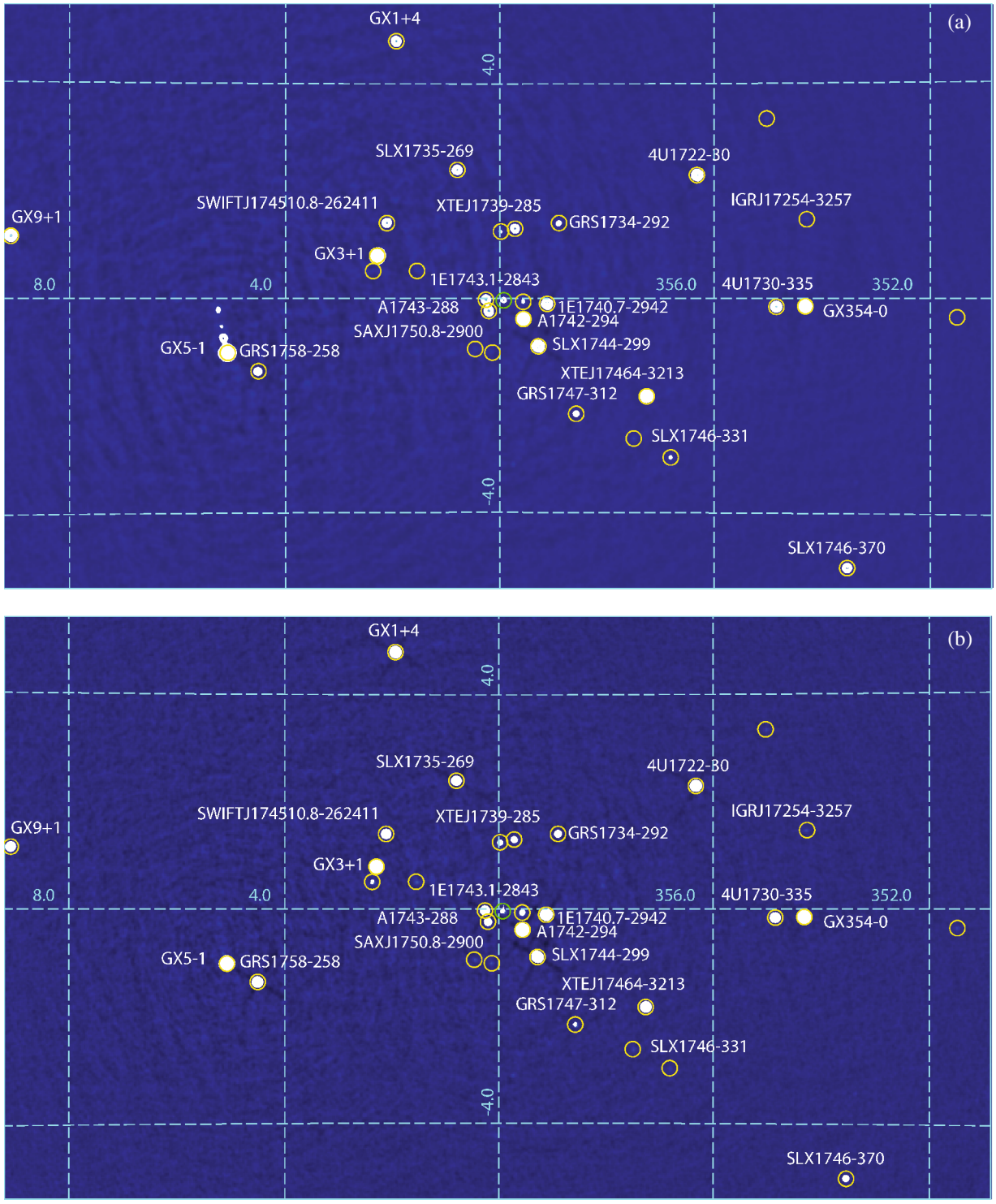

Fig. 2. (Color online) Integral S/N maps for the central Galactic region in the 5–10 (a) and 10–25 keV (b) energy bands smoothed with a Gaussian of 3′ in radius. The white contours with a logarithmic step indicate the S/N levels starting from 6σ.

in the sky region being studied; besides, an intense diffuse Galactic ridge X-ray emission is present (e.g., Krivonos et al. 2007). The addition of errors resulted, even despite of smoothing, in background inhomogeneities (systematic noise) in the reconstructed integral image (Fig. 2), which severely limited the possibility of searching for previously unknown faint sources in the field. The systematic noise is particularly strong in the soft X-ray image. On average over the entire field, it turned out that such noise did

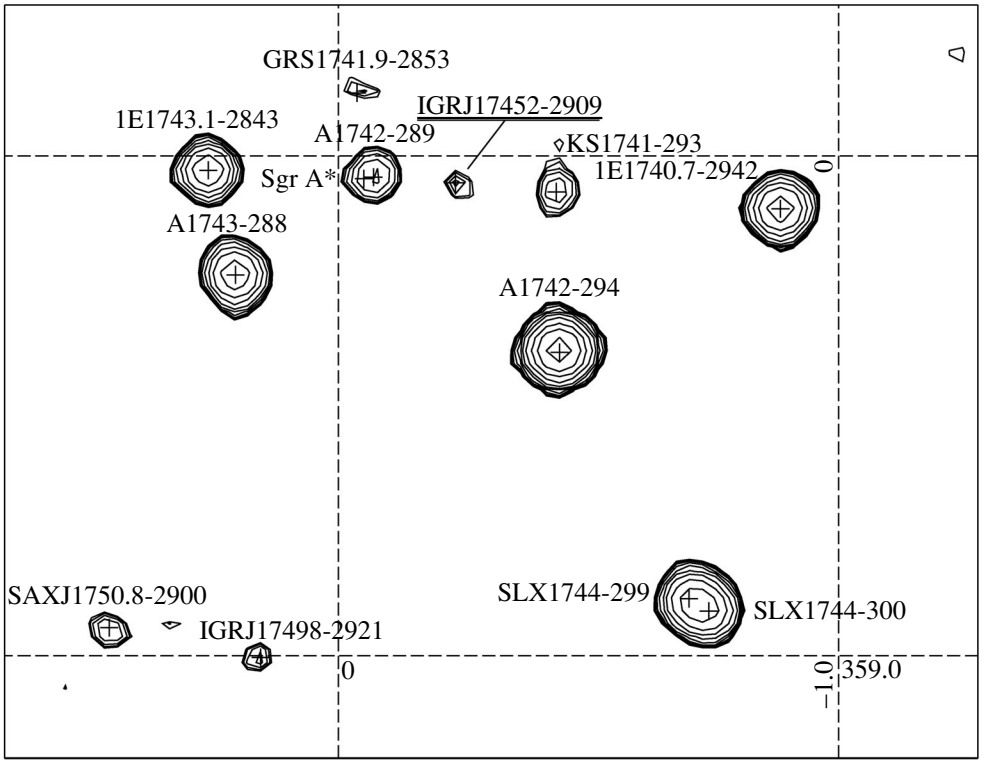

Fig. 3. Map of the central 2°.0 × 1°.5 of the Galactic region in the 5–10 keV energy band. The contours are given at $S/N = 6.0$, 6.4, 7.1, 8.4, 11, 15, 22, ...σ (with a logarithmic step). The previously unknown source IGR J17452-2909 was detected with $S/N = 9.2$.

not allow a sensitivity better than ∼2 mCrab to be achieved, although the long accumulated exposure theoretically allowed this to be done. The best sensitivity was ≈0.8 mCrab in the vicinity of SLX 1746-331. The worst sensitivity, 8–10 mCrab, was near the brightest soft X-ray source GX 5-1 (note the chain of false sources in its vicinity in Fig. 2a).

The S/N map in the 5–10 keV energy band for the innermost Galactic region (an enlarged cut from the corresponding map in Fig. 2 but without convolution with a Gaussian) is shown in Fig. 3. The well-known bright sources A1742-294, 1E1740.7-2942, SLX 1744-299/SLX 1744-300, 1E1743.1-2843, and A1743-288 (=SAX J1747-2853), the fainter GRS 1741.9-2853, KS 1741-293, SAX J1750.8-2900, and IGR J17498-2921, and the previously unknown source IGR J17452-2909 are clearly seen. The latter source was detected at $S/N = 9.2$ in the soft X-ray 5–10 keV image (and only at $S/N = 4.3$ in the hard one). There are no more unidentified excesses above the noise of comparable significance (actually, there are no excesses above $S/N \simeq 7$) in the field. However, given the complex background systematics, we still cannot be absolutely sure that this source is real. It would be more correct to call IGR J17452-2909 a candidate for a new source.

SLX 1744-299 and SLX 1744-300 are at a projected angular distance of ∼2′.5 from each other and cannot be resolved by the JEM-X telescope. Nevertheless, it can be clearly seen that the signal excess above the background corresponding to these sources in Fig. 3 has an elongated shape along the line connecting their positions. Obviously, the sources make approximately equal contributions to the observed total emission. The situation with A 1742-289, which is only at 75″ from the Galactic nucleus, the radio source Sgr A*, is similar. Here, the shape of the signal excess above the background in the image is also distorted but to a considerably lesser extent than in the case of SLX 1744-299 and SLX 1744-300; the emission from Sgr A* contributes only slightly to the emission from the X-ray burster A 1742-289.

The Catalog

We detected 83 sources on the integral sky maps obtained over the entire time of observations within 20° of the Galactic center and 22 more sources in the images obtained in individual pointings or in the integral images corresponding to individual revolutions. Except for the already mentioned IGR J17452-2909, they were all known previously. Most of the

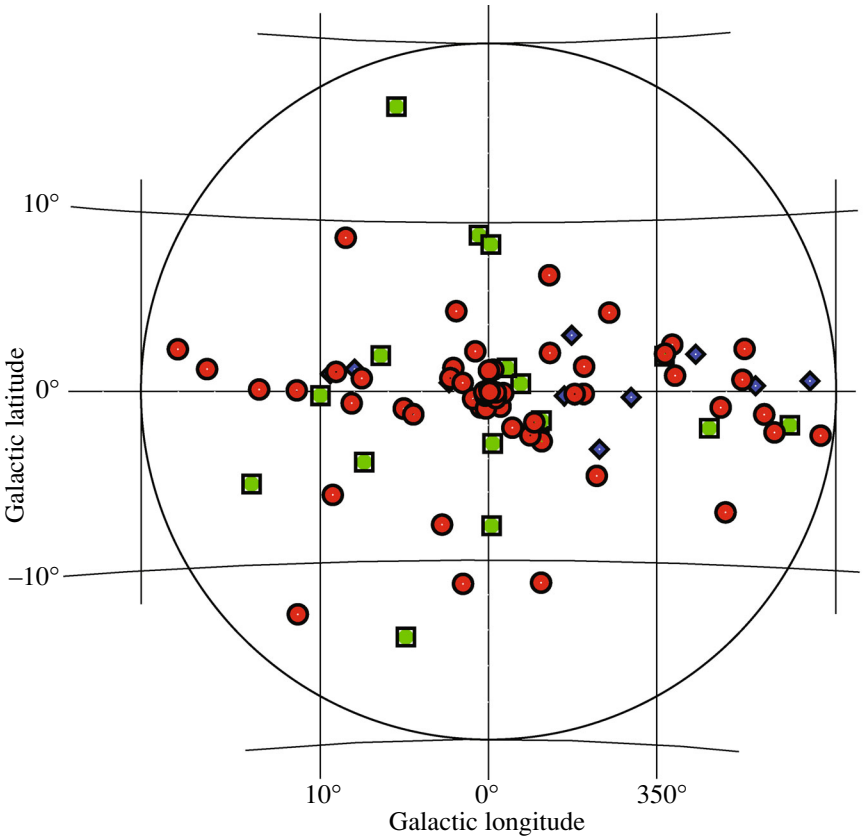

Fig. 4. (Color online) Distribution of detected sources of various types over the field: LMXBs (circles), HMXBs (squares), AGNs and other sources (diamonds). It can be seen that some of the LMXBs have a strong concentration to the Galactic center; the remaining LMXBs and HMXBs concentrate to the Galactic plane.

sources are Galactic X-ray binary systems: 73 low-mass X-ray binaries (LMXBs), 18 high-mass X-ray binaries (HMXBs), and 3 cataclysmic variables (CVs). Obviously, XTE J1652-453 whose observational manifestations are close to the properties of X-ray novae, which allows it to be considered as a black hole candidate, is also a binary system, most likely a LMXB. The X-ray burster XTE J174457-2850.3 is probably also a LMXB member, although its properties are not quite typical for objects of this type (Degenaar et al. 2014). Thus, on the whole, the catalog contains 96 X-ray binaries. The type of some (4) sources has not yet been determined. Apart from IGR J17452-2909, 1RXS J175721.2-304405 has been detected for the first time in the standard X-ray band. Previously, it was observed only at very low energies $\leq$2 keV. The extragalactic sources are represented by three active galactic nuclei (AGNs) and the galaxy cluster in Ophiucus (Oph CL). The distribution of sources of various types over the field is shown in Fig. 4. It can be seen that many of the LMXBs exhibit a strong concentration to the Galactic center, while some of the LMXBs and HMXBs are scattered along and near the Galactic plane, where regions of active star formation are located in the Galactic arms.

The complete catalog of 105 sources is given in Tables 1 (the quasi-persistent ones detected on the integral mosaics) and 2 (the transients detected only in the images corresponding to individual revolutions). The sources are listed in order of increasing right ascension (epoch 2000.0). The averaged fluxes in mCrab in the 5–10 and/or 10–25 keV energy bands are given for all sources; the fluxes corresponding to the greatest detection significance with an indication of the revolution are given for the sources that were detected only in individual revolutions and that are absent on the integral map. The Galactic coordinates of the sources based on JEM-X data and their deviation in arcmin from the source position in the INTEGRAL General Reference Catalog, V.31 (Ebisawa et al. 2003), are also provided.

The Distribution of Sources in the Galaxy

The Galaxy is transparent to X-rays in the fairly hard, $h\nu \gtrsim 5$ keV, energy band of the JEM-X telescope. As far as its sensitivity allows, the telescope

Table 1. Persistent sources (detected on the integral sky maps)

No.	Source	Flux, mCrab		l^a	b^a	Δ^a	Type[b]
		5–10 keV	10–25 keV	deg	deg	arcsec	
1	IGR J16493-4348	1.78 ± 0.22	1.91 ± 0.27	341.384	0.588	0.58	HMXB
2	MAXI J1659-152	34.34 ± 0.32	53.36 ± 0.56	5.516	16.526	0.03	LMXB/BH
3	GRO J1655-40	17.96 ± 0.21	8.71 ± 0.29	344.982	2.457	0.11	LMXB/BH
4	OAO 1657-415	14.52 ± 0.20	31.6 ± 0.27	344.369	0.319	0.23	HMXB
5	XTE J1701-462	16.3 ± 0.21	10.31 ± 0.22	340.813	−2.489	0.32	LMXB
6	XTE J1701-407	7.51 ± 0.17	5.49 ± 0.19	345.105	0.672	0.5	LMXB
7	4U 1700-377	96.73 ± 0.43	144.6 ± 0.52	347.754	2.174	0.26	HMXB
8	XTE J1704-445	2.46 ± 0.16	–	342.479	−1.925	0.52	–
9	GX 349+2	793.02 ± 1.02	362.05 ± 0.49	349.103	2.749	0.23	LMXB
10	4U 1702-429	50.08 ± 0.24	31.04 ± 0.29	343.887	−1.319	0.28	LMXB
11	4U 1705-32	2.62 ± 0.22	2.31 ± 0.3	352.792	4.675	1.03	LMXB
12	H 1705-440	219.91 ± 0.35	112.59 ± 0.38	343.321	−2.342	0.17	LMXB
13	IGR J17091-3624	26.64 ± 0.38	18.09 ± 0.38	349.524	2.215	0.28	LMXB/BH
14	IGR J17098-3628	3.26 ± 0.34	–	349.554	2.074	0.04	LMXB/BH
15	XTE J1710-281	2.27 ± 0.20	2.71 ± 0.36	356.36	6.919	0.33	LMXB
16	4U 1708-40	41.28 ± 0.20	14.1 ± 0.25	346.329	−0.929	0.31	LMXB
17	Oph Cluster	3.80 ± 0.24	2.91 ± 0.23	0.581	9.281	0.53	CL
18	SAX J1712.6-3739	8.10 ± 0.31	6.76 ± 0.32	348.941	0.924	0.44	LMXB
19	V2400 Oph	2.78 ± 0.21	3.74 ± 0.31	359.865	8.738	0.16	CV
20	IGR J17195-4100	1.77 ± 0.19	2.45 ± 0.18	346.979	−2.135	0.22	CV
21	IGR J17200-3116	1.74 ± 0.14	2.07 ± 0.19	355.022	3.346	0.06	HMXB
22	IGR J17252-3616	3.36 ± 0.16	7.61 ± 0.23	351.498	−0.353	0.2	HMXB
23	IGR J17254-3257	2.15 ± 0.12	2.04 ± 0.17	354.283	1.474	0.52	LMXB
24	4U 1722-30	24.03 ± 0.12	22.3 ± 0.17	356.32	2.298	0.21	LMXB
25	4U 1728-169	290.18 ± 0.93	125.66 ± 0.64	8.511	9.037	0.43	LMXB
26	GX 354-0	127.17 ± 0.16	101.06 ± 0.24	354.304	−0.150	0.28	LMXB
27	GX 1+4	18.10 ± 0.14	35.97 ± 0.24	1.936	4.794	0.22	LMXB
28	4U 1730-335	15.97 ± 0.11	11.7 ± 0.15	354.842	−0.160	0.1	LMXB
29	IGR J17354-3255	1.15 ± 0.11	1.06 ± 0.12	355.460	−0.268	0.26	HMXB
30	GRS 1734-292	2.99 ± 0.09	4.34 ± 0.17	358.894	1.405	0.13	AGN
31	SLX 1735-269	10.52 ± 0.11	10.59 ± 0.15	0.796	2.399	0.3	LMXB
32	4U 1735-444	224.58 ± 0.54	141.84 ± 0.45	346.055	−6.993	0.26	LMXB
33	IGR J17391-3021	0.96 ± 0.08	0.86 ± 0.10	358.066	0.454	0.51	SFXT
34	XTE J1739-285	4.22 ± 0.10	2.6 ± 0.09	359.716	1.300	0.17	LMXB
35	2E 1737.5-2817	2.40 ± 0.10	2.99 ± 0.13	359.980	1.248	0.16	LMXB
36	XTE J1743-363	1.26 ± 0.15	1.65 ± 0.21	353.373	−3.427	0.26	HMXB
37	1E 1740.7-2942	15.25 ± 0.10	23.44 ± 0.16	359.116	−0.106	0.23	LMXB
38	IGR J17448-3232	0.60 ± 0.10	–	356.825	−1.731	1.98	SNR + AGN
39	KS 1741-293	1.16 ± 0.09	1.71 ± 0.11	359.564	−0.067	0.53	LMXB
40	GRS 1741.9-2853	0.93 ± 0.10	0.66 ± 0.12	359.958	0.132	1.24	LMXB
41	SWIFTJ174510.8-262411	14.03 ± 0.16	13.01 ± 0.15	2.112	1.403	0.06	LMXB/BH
42	A 1742-289	2.76 ± 0.14	2.0 ± 0.12	359.929	−0.040	0.04	LMXB

Table 1. (Contd.)

No.	Source	Flux, mCrab		l^a	b^a	Δ^a	Type[b]
		5–10 keV	10–25 keV	deg	deg	arcsec	
43	A 1742-294	45.42 ± 0.13	31.3 ± 0.17	359.559	−0.389	0.29	LMXB
44	IGR J17452-2909	0.84 ± 0.09	0.52 ± 0.12	359.776	−0.054	1.0	–
45	XTE J17464-3213	24.59 ± 0.13	13.68 ± 0.15	357.255	−1.832	0.27	LMXB/BH
46	1E 1743.1-2843	11.07 ± 0.12	8.6 ± 0.15	0.262	−0.029	0.08	LMXB
47	A 1743-288	9.48 ± 0.11	4.25 ± 0.12	0.206	−0.238	0.33	LMXB
48	IGR J17473-2721	–	1.64 ± 0.14	1.550	0.510	0.14	LMXB
49	SLX 1744-299[c]	17.76 ± 0.10	11.9 ± 0.12	359.280	−0.899	0.26	LMXB
50	SLX 1744-300[c]	–	–	–	–	–	LMXB
51	GX 3+1	314.56 ± 0.31	123.5 ± 0.32	2.293	0.793	0.21	LMXB
52	IGR J17488-3253	–	0.98 ± 0.15	356.957	−2.666	0.26	AGN
53	GRO J1750-27	–	2.83 ± 0.15	2.371	0.507	0.14	HMXB
54	IGR J17497-2821	–	0.91 ± 0.12	0.929	−0.439	0.93	LMXB
55	SLX 1746-331	3.02 ± 0.09	1.07 ± 0.15	356.808	−2.972	0.07	LMXB
56	IGR J17498-2921	1.25 ± 0.14	1.45 ± 0.12	0.158	−1.008	0.3	LMXB
57	1E 1746.7-3224	1.58 ± 0.09	1.05 ± 0.14	357.498	−2.620	0.73	LMXB
58	SLX 1746-370	37.63 ± 0.18	20.78 ± 0.28	353.531	−5.005	0.33	LMXB
59	SAX J1750.8-2900	1.34 ± 0.10	1.19 ± 0.12	0.463	−0.949	0.44	LMXB
60	GRS 1747-312	3.36 ± 0.10	2.7 ± 0.13	358.573	−2.161	0.19	LMXB
61	XTE J1752-223	–	1.48 ± 0.27	6.443	2.133	2.61	LMXB/BH
62	1RXSJ175721.2-304405	1.76 ± 0.14	0.95 ± 0.14	359.751	−3.105	0.12	LMXB
63	IGR J17586-2129	3.34 ± 0.30	2.55 ± 0.30	7.990	1.317	0.61	HMXBc
64	IGR J17597-2201	7.13 ± 0.41	4.68 ± 0.32	7.568	0.776	0.08	LMXB
65	GX 5-1	1085.94 ± 1.11	413.19 ± 0.55	5.078	−1.018	0.29	LMXB
66	GRS 1758-258	21.41 ± 0.42	33.35 ± 0.35	4.507	−1.361	0.18	LMXB
67	GX 9+1	642.95 ± 0.79	262.8 ± 0.39	9.076	1.153	0.29	LMXB
68	IGR J18027-2016	3.5 ± 0.36	7.56 ± 0.33	9.419	1.038	0.59	HMXB
69	SAX J1806.5-2215	–	2.41 ± 0.40	8.162	−0.698	1.13	LMXB
70	SGR 1806-20	2.57 ± 0.28	1.98 ± 0.25	9.990	−0.242	0.28	SGR
71	XTE J1810-189	2.73 ± 0.38	3.74 ± 0.28	11.363	0.058	0.43	LMXB
72	GX 13+1	366.6 ± 0.5	116.36 ± 0.43	13.516	0.108	0.16	LMXB
73	4U 1812-12	18.37 ± 0.29	23.87 ± 0.35	18.033	2.398	0.4	LMXB
74	GX 17+2	771.78 ± 1.11	375.4 ± 0.63	16.432	1.278	0.23	LMXB
75	XTE J1817-330	20.45 ± 0.24	15.20 ± 0.23	359.819	−7.994	0.25	LMXB/BH
76	XTE J1818-245	2.15 ± 0.29	–	7.423	−4.180	1.47	LMXB/BH
77	H 1820-303	306.22 ± 0.68	199.38 ± 0.54	2.788	−7.913	0.13	LMXB
78	4U 1822-371	36.21 ± 0.29	50.25 ± 0.49	356.850	−11.291	0.15	LMXB
79	GS 1826-24	53.93 ± 0.20	71.45 ± 0.36	9.272	−6.088	0.31	LMXB
80	MAXI J1836-194	4.21 ± 0.20	5.54 ± 0.37	13.948	−5.356	0.16	LMXB/BH
81	4U 1832-330	6.52 ± 0.28	8.86 ± 0.39	1.532	−11.370	0.25	LMXB
82	V1223 Sgr	5.12 ± 0.27	6.9 ± 0.68	4.953	−14.354	0.27	CV
83	HETE J1900.1-2455	21.15 ± 0.28	26.6 ± 0.40	11.303	−12.874	0.36	LMXB

[a] Galactic coordinates and the deviation from the adopted position.

[b] LMXB — low-mass X-ray binary, HMXB — high-mass X-ray binary, SFXT—supergiant fast X-ray transient, CV—cataclysmic variable, BH—black hole candidate, SGR—soft gamma repeater, AGN—active galactic nucleus, HMXBe—high-mass X-ray Be binary, CL—galaxy cluster.

[c] Two close unresolved sources; the fluxes and coordinates are given for their total emission.

Table 2. Transients detected only during outbursts

No.	Source	Flux[a], mCrab		l^b	b^c	Δ^b	Type[c]	Revolution[d]
		5–10 keV	10–25 keV	deg	deg	arcsec		
1	IGRJ16465-4507	16.55 ± 2.10	18.36 ± 1.59	340.049	0.132	1.24	SFXT	232
2	XTEJ1652-453	27.08 ± 2.28	31.35 ± 2.36	340.527	−0.793	0.4	XB/BH	844
3	XTEJ1709-267	42.1 ± 1.83	–	357.469	7.911	0.22	LMXB	173
4	4U1711-34	–	38.02 ± 3.29	352.057	2.752	0.92	LMXB	896
5	XTEJ1716-389	46.94 ± 4.35	–	348.341	−0.332	0.72	HMXB	60
6	XTEJ1720-318	18.67 ± 2.09	21.90 ± 3.15	354.616	3.095	0.58	LMXB	58
7	IGR J17419-2802	–	11.38 ± 1.01	0.343	1.162	0.49	–	362
8	XMMUJ 174445.5-295044	10.04 ± 1.02	15.75 ± 1.12	359.126	−0.313	0.12	–	1217
9	XMM J174457-2850.3	10.43 ± 1.36	–	0.010	0.172	0.22	XB/NS	1200
10	IGR J17480-2446	722.73 ± 4.62	395.90 ± 3.45	3.842	1.687	1.30	LMXB	978
11	A1744-361	73.24 ± 2.09	42.08 ± 3.34	354.118	−4.194	0.46	LMXB	1088
12	AX J1749.1-2733	–	12.44 ± 1.18	1.601	0.070	0.62	HMXB	110
13	2XMM J174931.6-280805	11.12 ± 1.41	12.42 ± 1.45	1.134	−0.315	0.40	LMXB	915
14	IGRJ17511-3057	24.75 ± 0.84	30.85 ± 1.15	358.880	−2.071	0.15	LMXB	846
15	XTEJ1751-305	11.88 ± 1.03	11.44 ± 1.08	359.182	−1.912	0.10	LMXB	546
16	AX J1754.2-2754	169.39 ± 10.93	77.8 ± 8.91	1.852	−1.105	0.32	LMXB	306
17	IGR J17544-2619	–	36.8 ± 3.46	3.242	−0.335	1.44	SFXT	171
18	SAXJ1808.4-3658	42.42 ± 2.54	46.32 ± 4.65	355.383	−8.147	0.27	LMXB	729
19	V4722 Sgr	56.15 ± 4.67	53.5 ± 4.28	5.192	−3.433	0.56	LMXB	604
20	SWIFT J1816.7-1613	–	17.09 ± 1.44	14.584	0.091	0.66	HMXB	668
21	IGR J18179-1621	–	40.96 ± 2.56	14.600	−0.219	0.15	HMXBe	1146
22	SAX J1818.6-1703	–	63.69 ± 5.68	14.087	−0.716	0.74	HMXB	411

[a] Mean photon flux from the source during the specified[d] satellite revolution.
[b] Galactic coordinates and the deviation from the adopted position.
[c] LMXB—low-mass X-ray binary, HMXB—high-mass X-ray binary, HMXBe—high-mass X-ray Be binary, SFXT—supergiant fast X-ray transient.
[d] Number of the INTEGRAL revolution during which the source's outburst occurred. The dates and times of observations can be found at www.cosmos.esa.int/web/integral/schedule-information.

can see all sources of certain brightness in it without noticeable distortions. Accordingly, the sample of detected sources can be used to analyze their spatial distribution. It is clear already from Fig. 4 that this distribution is characterized by a strong concentration to the Galactic center. The optical and infrared stars are also concentrated to the center, so that, at first glance, this comes as no surprise. In reality, however, since the period of X-ray activity is short, the distribution of X-ray sources must be sensitive to the age of the stellar population in the Galactic region under consideration, and, therefore, it can differ greatly from the stellar mass distribution. It is interesting to compare these distributions quantitatively.

The first attempt at such a comparison was made by Grebenev et al. (1996) based on the survey of the Galactic center region with the ART-P telescope onboard the GRANAT observatory. This telescope was similar in many parameters to the JEM-X telescope. Seventeen sources were detected in the $8^\circ \times 8^\circ$ field. The growth of their surface density toward the Galactic center was shown to agree, in general, with the stellar mass distribution. Subsequently, as new sources were detected in this region and as our

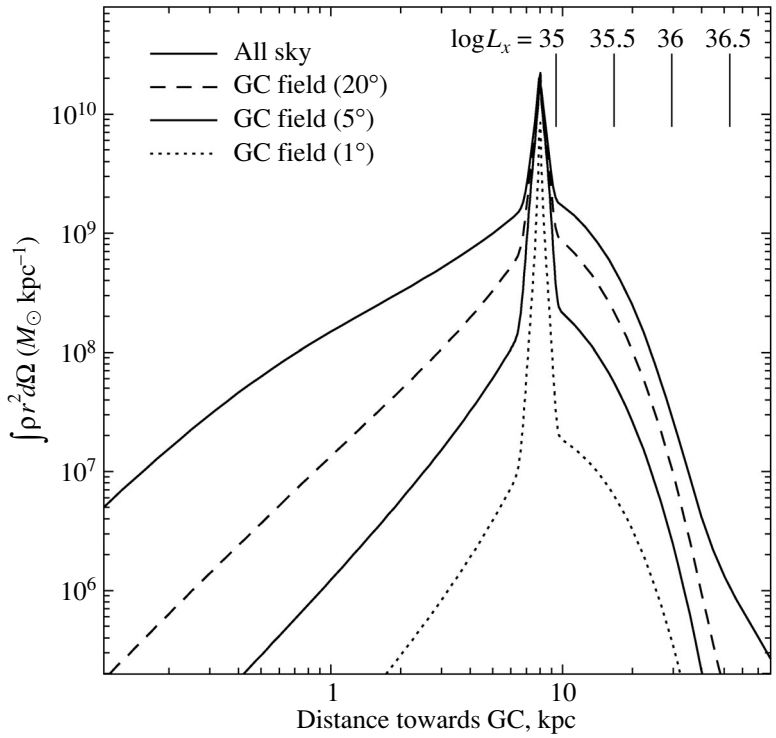

Fig. 5. Stellar mass toward the Galactic center as a function of the distance and field of view (the entire sky, the fields with a radius of 20°, 5°, and 1°). The vertical lines indicate the limiting distances at which a source with a 5–10 keV luminosity L_X can be detected by a telescope with a sensitivity threshold of ∼1 mCrab.

knowledge of their distances were improved, such studies have been repeated and perfected more than once (e.g., Grimm et al. 2002; Lutovinov et al. 2005a; Revnivtsev et al. 2008). Nevertheless, an analysis based on JEM-X data is not meaningless. Owing to the unprecedentedly long observations, the large investigated field, the good angular resolution, the high sensitivity, and even simply the X-ray band intermediate between the bands of the telescopes with grazing-incidence mirrors and hard X-ray telescopes of the INTEGRAL and SWIFT observatories, the set of sources detected by JEM-X is unique and in many respects more perfect and complete than those used previously.

The sample of LMXBs in the survey with highly evolved stars as their optical companions are of greatest interest. LMXBs dominate among the sources in the survey (75 of the 105 sources), reflecting that they belong to the Galactic bulge populated by old stars and occupying its central kiloparsec. Our survey completely covers the bulge (1 kpc at the distance of the Galactic center 8 kpc corresponds to ∼7°). Figure 5 shows the density distribution of the stellar mass visible by the telescope toward the Galactic center as a function of the distance and the width of the field of view (the entire sky or the regions with a radius of 20°, 5°, and 1°). We used the three-component Bahcall–Soneira (BS) model of the distribution of visible stellar mass in the Galaxy that includes a disk, a spheroid, and a central bulge (Bahcall and Soneira 1980; Bahcall 1986). By no means the entire mass of the Galaxy is associated with stars: in the central regions, they account for only ∼1/3 of the mass; the rest is accounted for by dark matter, interstellar gas and dust. We are interested precisely in the stellar mass. In the region with a radius of 20°, we see an appreciable (∼68%) fraction of the mass of all stars in the Galaxy: 100% of the bulge mass ($\simeq 1.4 \times 10^{10}\ M_\odot$), 56% of the spheroid mass ($\simeq 9 \times 10^8\ M_\odot$), and 40% of the disk mass ($\simeq 8 \times 10^9\ M_\odot$).

The limits of the JEM-X sensitivity to sources of various 5–10 keV luminosities are shown in the upper part of Fig. 5. We assumed the minimum flux confidently recorded by the telescope to be 1 mCrab and the spectrum of sources to be similar to that of the Crab pulsar; the interstellar extinction was neglected. Obviously, the telescope sees almost all X-ray objects toward the Galactic center that fell within the field of view with a luminosity exceeding 10^{36} erg s^{-1} and only slightly more than half of the sources with a luminosity $\sim 10^{35}$ erg s^{-1}.

Figure 6a shows the surface number density distribution of LMXBs from the catalog as a function of their projected distance from the Galactic center. For comparison, the distribution predicted by the BS model under the assumption that 150 active low-

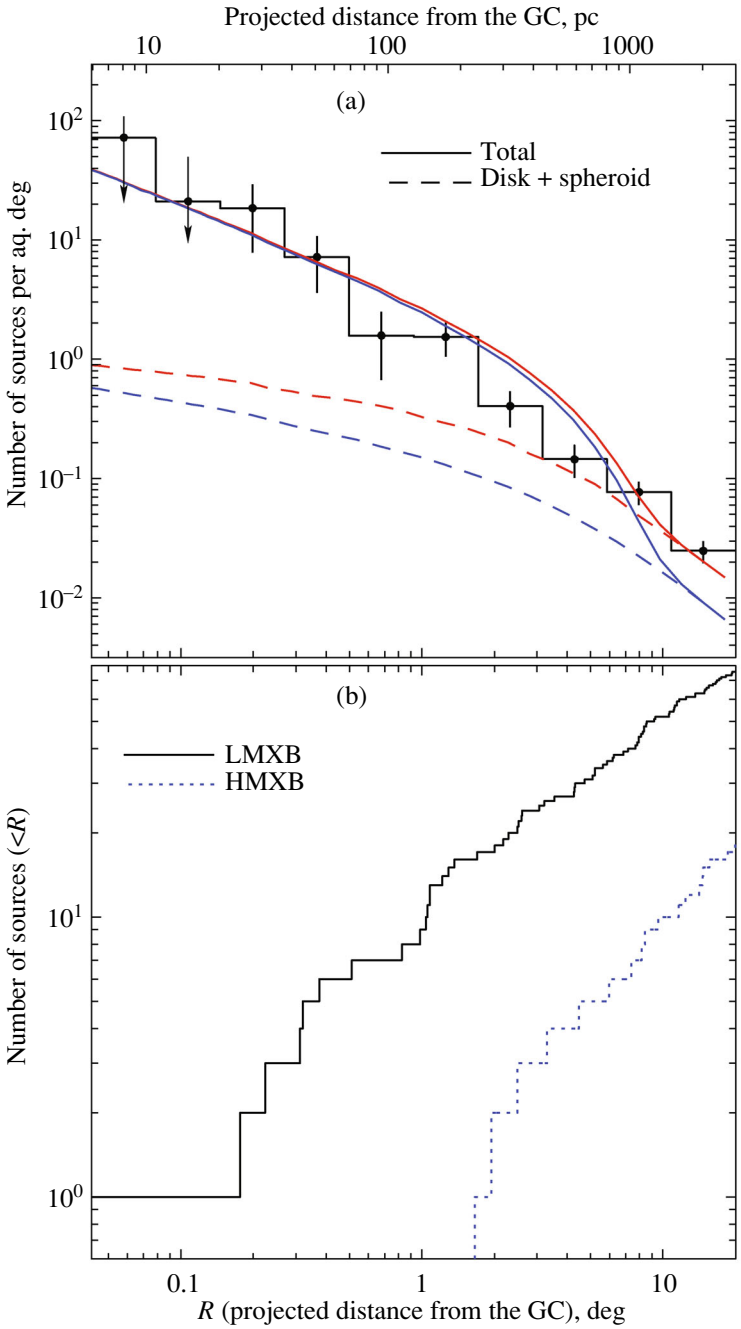

Fig. 6. (Color online) (a) The distribution of 75 LMXBs detected by JEM-X in their projected distance from the Galactic center R. The solid lines indicate the predictions of the BS model for the distribution of sources with 5–10 keV luminosities of 1×10^{37} (upper/red curve) and 1×10^{35} erg s^{-1} (lower/blue curve) under the assumption that, on average, there is one low-mass X-ray source per 2.2×10^8 $M_\odot$ stellar mass in the Galaxy. The dashed lines indicate the fraction of X-ray sources contained in the stellar disk and spheroid. (b) The cumulative distribution of these LMXBs (solid histogram) in comparison with that of 18 HMXBs detected in the survey.

mass X-ray systems (one system per 2.2×10^8 $M_\odot$)[2] act in the Galaxy is presented. The distributions agree satisfactorily between themselves, although a slight deficit of real sources is observed at distances of 70–700 pc from the Galactic center. The predicted distribution depends on the luminosity of sources due to the limited sensitivity of the telescope ($\simeq$1 mCrab). The luminosity in the 5–10 keV energy band was assumed to be 1×10^{37} (upper red curves) or $1 \times$

[2] There is assumed here that LMXB systems are distributed uniformly over the entire mass of the Galaxy, that is wrong, of course. But if we fall to another extreme and assume that they all are located in the bulge, their total number will be restricted by ~64, that is also obviously wrong.

10^{35} erg s^{-1} (lower blue curves). The fraction of sources contained in the disk and the spheroid is indicated by the dashed lines. Obviously, as the luminosity decreases, the faint sources of precisely these Galactic structure components cease to be observed, while all sources of the Galactic bulge are detected with confidence down to luminosities of 1×10^{35} erg s^{-1}.

The lower panel in Fig. 6 presents the cumulative distribution of LMXBs as a function of their projected distance from the Galactic center. The analogous distribution of HMXBs from the catalog is also presented. It can be seen that there is no HMXB within 230 pc of the Galactic center.

The Luminosity Function of LMXBs

The most important characteristic of a population of sources is their luminosity distribution in a certain energy band (luminosity function). In the X-ray band, after the appearance of the highly sensitive CHANDRA and XMM telescopes with grazing-incidence mirrors, the X-ray luminosity functions were measured for sources in many nearby galaxies (Gilfanov 2004; Kim and Fabbiano 2004). Our Galaxy, for which the construction of the luminosity function is complicated by poor knowledge of the distances to many sources, the large angular size of the Galaxy, the highly nonuniform coverage of its field by observations, and appreciable interstellar extinction in the Galactic plane, turned out to be the most difficult case. Nevertheless, attempts to construct its luminosity function have been made (e.g., Grimm et al. 2002; Revnivtsev et al. 2008).

A common problem in investigating the luminosity distribution of X-ray sources in our and other galaxies is their strong variability to the point of being transient, when the usually "switched-off" sources become bright for a short period of time. As a rule, the duration of the observations of an individual sky field by the CHANDRA and XMM telescopes does not exceed several kiloseconds; therefore, an appreciable number of transients detected at the time of outbursts or variable sources with a luminosity differing greatly from the mean one are inevitably present in the population of sources found by them. The long (more than ten years) duration of the JEM-X sky survey provides a unique opportunity to separate persistent X-ray sources from transients and to construct the persistent X-ray luminosity function of the Galaxy for the first time. As has already been noted, primarily the LMXBs, whose population is represented in our survey fairly completely, are of interest here.

Only half (31 binaries, see Table 3) of the 62 LMXBs in Table 1 confidently detected by JEM-X on the integral sky maps may be considered as "relatively persistent" X-ray sources; the rest (Table 4) are highly variable sources that were detected more or less regularly by JEM-X (for example, H 1705-440 or GX 1+4) or that experienced one long (several months) or several short (at different times) outbursts. By "highly variable" here we mean the binaries whose brightness in individual revolutions (on a time scale of $\sim$3 days) exceeded appreciably (by a factor of 5 or more) the mean one. For faint binaries, which were not detected by JEM-X at a statistically significant level in individual revolutions, the absence of outbursts was checked using the light curves measured on long time scales by the ASM/RXTE all-sky monitor and the IBIS/ISGRI/INTEGRAL telescope. The fraction of the time during which the transients from Table 4 were in an active state during their observations with JEM-X is given in column 5 of Table 4. Even if the characteristic period of outbursts for a transient is short compared to the duration of the survey, its mean luminosity is still an important physical parameter characterizing the accretion process in the binary, and, therefore, it can be used to construct another luminosity function, for Galactic transients.

For most of the sources from Tables 3 and 4, the distances are known with a satisfactory accuracy (better than 30%); for the remaining ones, IGR J17254-3257, 2E 1737.5-2817, KS 1741-293, GRS 1741.9-2853, A 1742-289, SLX 1744-300, SLX 1746-331, 1E 1746.7-3224, 1RXS J175721.2-304405, SAX J1806.5-2215, XTE J1810-189, and MAXI J1836-194, they were set equal to the distance from the Galactic center, 8 kpc (in view of their proximity to the center in the plane of the sky). The adopted distances and corresponding mean luminosities of the sources being studied in the most interesting 5–10 keV energy band can be found in Tables 3 and 4.

The X-ray luminosity function in the 5–10 keV energy band for the Galactic population of persistent LMXBs constructed from these data is indicated in Fig. 7 (upper panel) by the filled circles. It agrees well with the model luminosity function of LMXBs in nearby late-type galaxies (solid line) constructed by Gilfanov (2004, see Fig. 10) from CHANDRA observations of galaxies:

$$L\frac{dN}{dL} = A_{br}\begin{cases}1, & \text{if } L < L_{br}\\ (L/L_{br})^{-\beta}, & \text{if } L > L_{br}\end{cases}. \quad (1)$$

The model luminosity function was normalized to the mass of the Galactic bulge, $\simeq 1.4 \times 10^{10}\ M_\odot$. Since the CHANDRA satellite is sensitive in the softer 0.5–8 keV X-ray band than the JEM-X one, the model luminosity function was recalculated by assuming the

Table 3. Adopted distances and luminosities of persistent LMXBs in the field

No.	Name	d^a, kpc	L_X^b, 10^{35} erg s^{-1}	Reference to distance
1	XTE J1701-407	5.0	1.8	Chenevez et al. (2010)
2	GX 349+2	8.5	550	Wachter and Margon (1996)
3	4U 1702-429	6.2	18.2	Jonker and Nelemans (2004)
4	4U 1705-32	13.0	4.2	in't Zand et al. (2005)
5	XTE J1710-281	17.3	6.5	Jonker and Nelemans (2004)
6	4U 1708-40	8.0	25.0	Migliari et al. (2003)
7	SAX J1712.6-3739	6.9	3.7	Jonker and Nelemans (2004)
8	IGR J17254-3257	8.0	1.3	
9	4U 1728-169	5.0	70.0	Christian and Swank (1997)
10	GX 354-0	5.3	34.0	Jonker and Nelemans (2004)
11	SLX 1735-269	8.5	7.2	Molkov et al. (2005)
12	4U 1735-444	9.4	190.0	Jonker and Nelemans (2004)
13	2E 1737.5-2817	8.0	1.5	
14	1E 1740.7-2942	8.5	10.0	White and van Paradijs (1996)
15	A 1742-294	8.1	28.0	Jonker and Nelemans (2004)
16	1E 1743.1-2843	8.0	6.8	Porquet et al. (2003)
17	SLX 1744-299	5.0	2.8	Li et al. (2008)
18	SLX 1744-300	8.0	3.6	
19	GX 3+1	5.0	75.0	Oosterbroek et al. (2001)
20	1E 1746.7-3224	8.0	0.96	
21	SLX 1746-370	11.0	43.3	Kuulkers et al. (2003)
22	GX 5-1	9.0	840	Jonker et al. (2000)
23	GRS 1758-258	8.0	13.0	Migliari et al. (2003)
24	GX 9+1	7.2	320	Christian and Swank (1997)
25	GX 13+1	7.0	170.0	Bandyopadhyay et al. (1999)
26	4U 1812-12	4.0	2.8	Jonker and Nelemans (2004)
27	GX 17+2	14.0	1400	Jonker and Nelemans (2004)
28	H 1820-303	7.6	170.0	Kuulkers et al. (2003)
29	4U 1822-371	2.5	2.1	Mason and Cordova (1982)
30	GS 1826-24	7.5	29.0	Kong et al. (2000)
31	4U 1832-330	9.6	5.7	Parmar et al. (2001)

[a] Distance to the source.
[b] Luminosity in the 5–10 keV band.

Table 4. Adopted distances and luminosities of transient LMXBs in the field (from the sources detected on the integral JEM-X maps)

No.	Name	d^a, kpc	L_X^b, 10^{35} erg s^{-1}	$\Delta t/T^c$, %	Reference to distance
1	MAXI J1659-152	8.6	24	8	Kuulkers et al. (2013)
2	GRO J1655-40	3.2	1.7	5	Jonker et al. (2004)
3	XTE J1701-462	8.8	12	8	Lin et al. (2009)
4	H 1705-440	8.4	150	60	Jonker et al. (2004)
5	IGR J17091-3624	14.0	50	10	Rodriguez et al. (2011)
6	IGR J17098-3628	10.5	3.4	10	Grebenev et al. (2007)
7	4U 1722-30	9.5	21	15	Kuulkers et al. (2003)
8	GX 1+4	4.5	3.5	35	Grimm et al. (2002)
9	4U 1730-335	8.8	12	20	Kuulkers et al. (2003)
10	XTE J1739-285	12.0	5.8	15	Torres et al. (2006)
11	KS 1741-293	8.0	0.71	5	
12	GRS 1741.9-2853	8.0	0.57	3	
13	SWIFTJ174510.8-262411	7.0	6.5	7	Munoz-Darias et al. (2013)
14	A 1742-289	8.0	1.7	10	
15	XTE J17464-3213	10.4	25	25	Corbel et al. (2005)
16	A 1743-288	7.5	5.1	15	Werner et al. (2004)
17	IGR J17473-2721	5.3	0.31	5	Altamirano et al. (2008)
18	IGR J17497-2821	8.0	0.50	2	Paizis et al. (2009)
19	SLX 1746-331	8.0	1.8	7	
20	IGR J17498-2921	7.6	0.68	2	Linares et al. (2011)
21	SAX J1750.8-2900	6.8	0.59	4	Galloway et al. (2008)
22	GRS 1747-312	9.5	2.9	15	Kuulkers et al. (2003)
23	XTE J1752-223	3.5	0.17	5	Shaposhnikov et al. (2010)
24	1RXSJ175721.2-304405	8.0	1.1	<1	
25	IGR J17597-2201	7.5	3.8	7	Lutovinov et al. (2005b)
26	SAX J1806.5-2215	8.0	1.6	15	
27	XTE J1810-189	8.0	1.7	6	
28	XTE J1817-330	2.5	1.2	7	Sala and Greiner (2006)
29	XTE J1818-245	3.5	0.25	8	Cadolle Bel et al. (2009)
30	MAXI J1836-194	8.0	2.6	6	
31	HETE J1900.1-2455	5.0	5.0	10	Kawai and Suzuki (2005)

[a] Distance to the source.
[b] Luminosity in the 5–10 keV band.
[c] Fraction of the active lifetime of the source (in %).

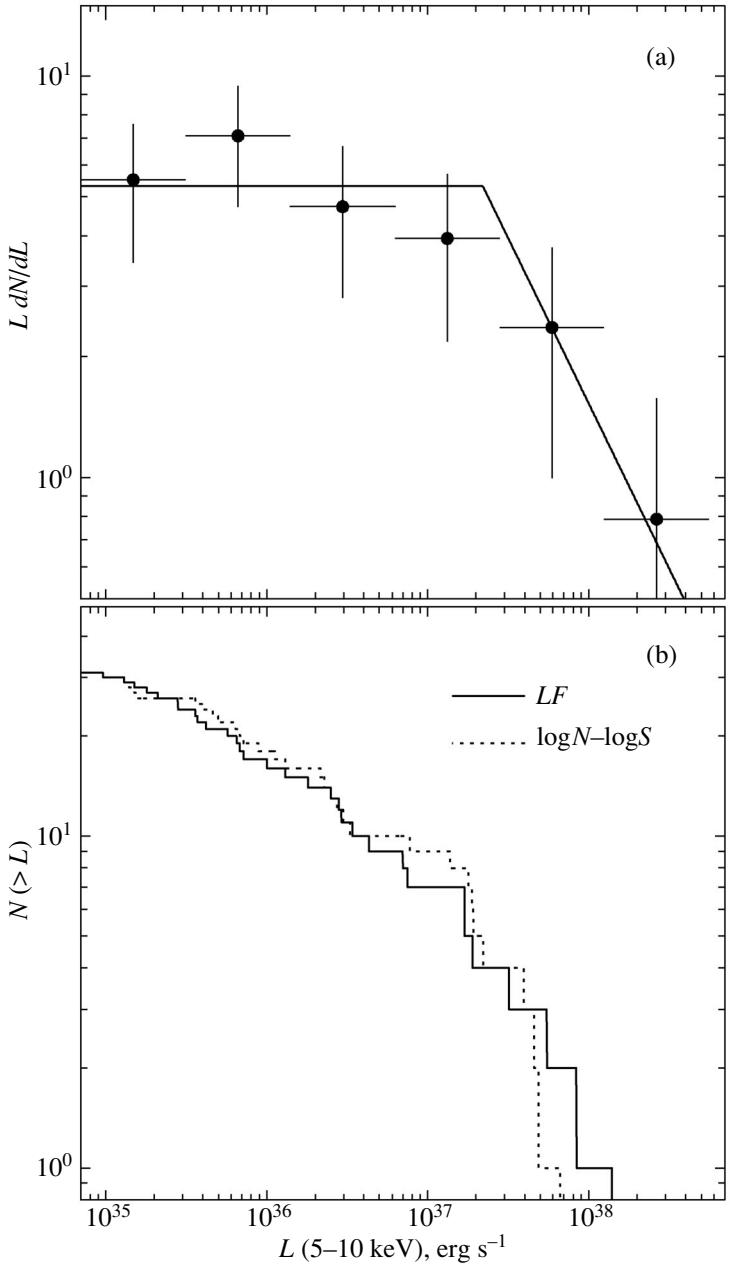

Fig. 7. Mean X-ray (5–10 keV) luminosity function of LMXBs detected by JEM-X in the Galactic center region in 2003–2013. (a) The differential luminosity function for all persistent sources; the solid line indicates the model luminosity function based on CHANDRA observations of several nearby galaxies (Gilfanov 2004) reduced to the JEM-X energy band and the mass of the Galactic bulge. (b) The cumulative luminosity function (solid line) in comparison with the curve $\log N - \log S$ (dashed line) assuming that all sources are at a distance of 8 kpc.

sources to have, on average, a power-law spectrum with a photon index $\alpha \simeq 1.65$. The parameters used for the presentation in Fig. 7 are $A_{br} \simeq 5.3$, $\beta = 0.82$, and $L_{br} = 2.2 \times 10^{37}$ erg s^{-1}. As we saw in the previous section, all sources of the Galactic bulge with a luminosity above $\sim 10^{35}$ erg s^{-1} must be visible for the JEM-X telescope; therefore, the selection effects may be neglected.

In the lower part of Fig. 7, the solid line indicates the cumulative mean X-ray luminosity function for the sample of persistent LMXBs and the dotted line indicates the curve $\log N - \log S$ for these sources (normalized by assuming that they are all at a distance of 8 kpc). When using the curve $\log N - \log S$,

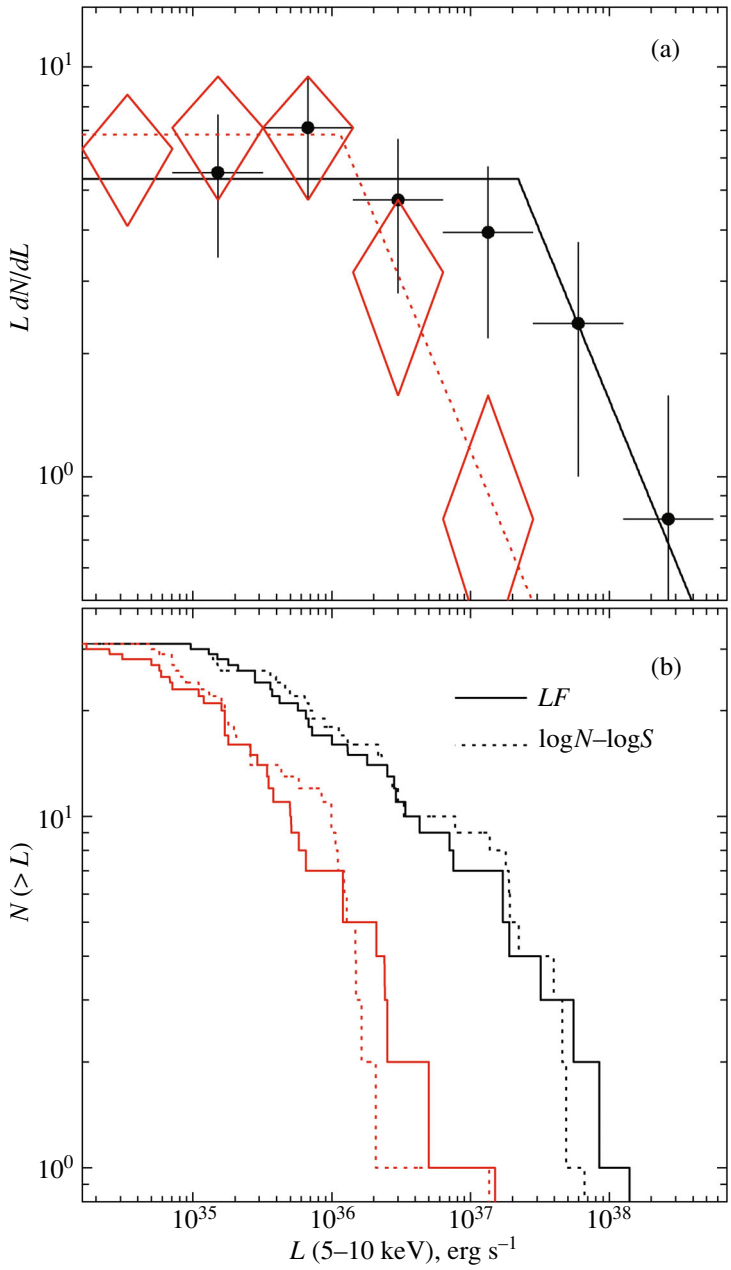

Fig. 8. (Color online) Mean X-ray (5–10 keV) luminosity function of LMXBs detected by JEM-X in the Galactic center region in 2003–2013. (a) The differential luminosity function for persistent sources (circles) and transients (diamonds); the solid line indicates the model luminosity function constructed from CHANDRA observations of several nearby galaxies, and the dashed line indicates the model fit to the luminosity function measured by JEM-X for transient LMXBs. (b) The cumulative luminosity functions (solid lines) for these groups of sources in comparison with the curves $\log N - \log S$ (dashed lines) assuming that all objects are at a distance of 8 kpc.

the number of bright ($L_X > 5 \times 10^{37}$ erg s^{-1}) sources turns out to be smaller than their actual number; these sources fall within the luminosity range $L_X \sim (0.5–1.5) \times 10^{37}$ erg s^{-1}.

It has been noted above that the sample of sources based on JEM-X data contains truly persistent objects (in contrast to the populations of sources obtained in the CHANDRA and XMM observations). It is interesting to check what contribution can be made by transients to the luminosity function when one galaxy is observed for a long time (as in the case of the JEM-X observation of our Galaxy) or during numerous observations of different galaxies (as in the case of the study performed by Gilfanov 2004).

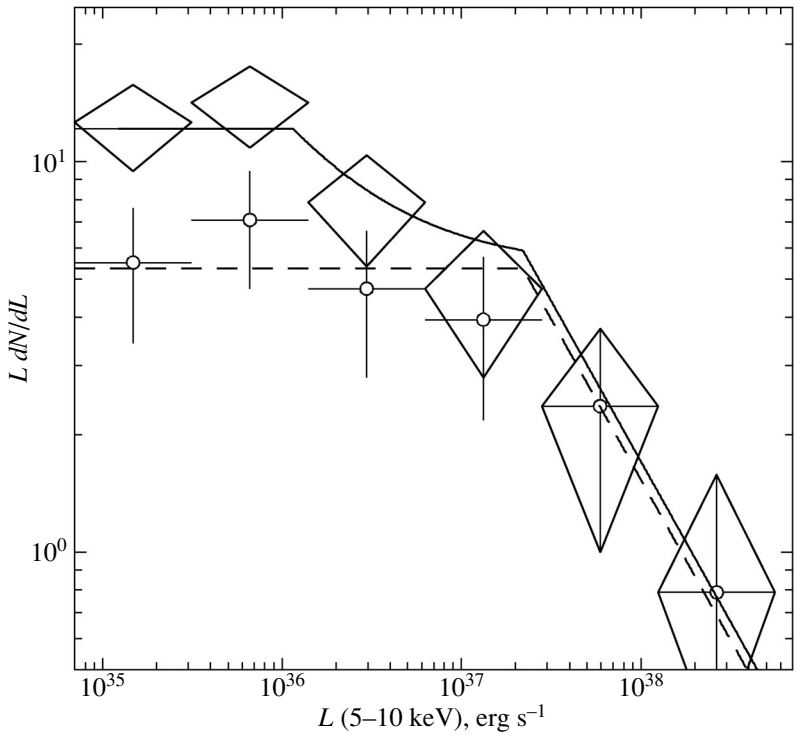

Fig. 9. Mean X-ray (5–10 keV) luminosity function of all LMXBs detected by JEM-X in the integral images of the Galactic center region (diamonds) in comparison with the luminosity function of only persistent sources (circles). The solid line indicates the sum of the model luminosity functions for persistent sources (dashed line) and transients.

Figure 8 shows the mean X-ray luminosity function (diamonds) in the same energy band for the sample of transients in the field (Table 4), along with the already described luminosity function of persistent sources. Although the statistics on these sources is not very large, it is clear that their luminosity function can be fitted by the same model function but shifted leftward to take into account the lower mean luminosity of transients and downward or upward to take into account the deviation of their number per unit mass of the bulge from the number of persistent sources. The fit by function (1) at the same $\beta = 0.82$ gives the following parameters: $A_{br} \simeq 6.8$ and $L_{br} \simeq 1.2 \times 10^{36}$ erg s^{-1}.

The cumulative mean X-ray luminosity functions for the samples of persistent and transient LMXBs are presented in the lower part of the figure in comparison; the dotted lines indicate the corresponding curves $\log N - \log S$ for these sources. Note that the curve $\log N - \log S$ differs from the luminosity function for transients much more strongly than that for persistent ones: there are much more bright objects located well beyond the Galactic center (at distances exceeding 8 kpc) among the transients; faint transients remain often unnoticed at such distances. Curiously, there are no objects with a luminosity below $L_X \sim 1 \times 10^{35}$ erg s^{-1} among the persistent sources of the sample, while such objects account for more than 30% among the transients. There may exist physical mechanisms that do not allow the sources with a low accretion rate to be persistent (stable).

CONCLUSIONS

A survey of the Galactic center region was performed in the two X-ray 5–10 and 10–25 keV energy bands using the JEM-X/INTEGRAL data. We compiled a catalog of detected sources and revealed the populations of quasi-persistent sources and X-ray transients. Most $(73 + 2)$ of the detected 105 sources are low-mass X-ray binaries (LMXBs). The mean luminosity functions were constructed for the populations of quasi-persistent and transient LMXBs in the standard X-ray band. We showed that the former agrees well with the model luminosity function following from the CHANDRA observations of nearby galaxies renormalized to the mass of the Galactic bulge, while the latter can be obtained from it by a shift along the luminosity axis and renormalization to the relative number of transients. During short scanning observations of the central region of the Galaxy (and other late-type galaxies), it is often impossible to

separate transients from persistent sources; therefore, their X-ray luminosity functions are added, which must lead to a distortion of the measured luminosity function for persistent sources at $L_X < 10^{37}$ erg s^{-1} due to an "artificial" increase in the number of faint sources. Figure 9 presents the luminosity function of all (persistent and transient) LMXBs detected by the JEM-X telescope in the integral images of the Galactic center field. It can be seen that at low luminosities, $L_X < 10^{37}$ erg s^{-1}, this luminosity function is no longer flat and differs significantly from the luminosity function of persistent sources. The solid line in the figure indicates the sum of the model functions fitting the mean luminosity functions of persistent and transient sources in the survey.

On the other hand, it is obvious that by no means all transients are detected in the CHANDRA and XMM surveys, and they cannot purport to completely take into account the population of X-ray sources when constructing the luminosity function. Our results may turn out to be important for solving the problem of the origin of the break near $L_{br} \simeq 10^{37}$ erg s^{-1} in the X-ray luminosity function of LMXBs in our and other galaxies (e.g., Postnov and Kuranov 2005; Revnivtsev et al. 2011; Kuranov et al. 2014). This break may be associated with the existence of a large number of X-ray transients with low mean luminosities, while there are virtually no persistent sources radiating in this luminosity range. The neglect of (or incomplete allowance for) X-ray transients when constructing the luminosity function must inevitably lead to a characteristic break, even if the initial luminosity function of X-ray binaries has a smooth, monotonic pattern.

ACKNOWLEDGMENTS

This work is based on the INTEGRAL observational data retrieved via the Russian and European science data centers of the observatory. The data analysis was financially supported by the Russian Science Foundation (project no. 14-22-00271).

REFERENCES

1. D. Altamirano, D. Galloway, J. Chenevez, J. in't Zand, E. Kuulkers, N. Degenaar, E. del Monte, M. Feroci, et al., Astron. Telegram 1651 (2008).
2. J. N. Bahcall and R. M. Soneira, Astrophys. J. Suppl. Ser. **44**, 73 (1980).
3. J. N. Bahcall, Ann. Rev. Astron. Astrophys. **24**, 577 (1986).
4. R. M. Bandyopadhyay, T. Shahbaz, P. A. Charles, and T. Naylor, Mon. Not. R. Astron. Soc. **306**, 417 (1999).
5. C. G. Bassa, P. G. Jonker, J. J. M. in't Zand, and F. Verbunt, Astron. Astrophys. **446**, L17 (2006).
6. A. J. Bird, A. Bazzano, L. Bassani, F. Capitanio, M. Fiocchi, A. B. Hill, A. Malizia, V. A. McBride, et al., Astrophys. J. Suppl. Ser. **186**, 1 (2010).
7. M. Cadolle Bel, L. Prat, J. Rodriguez, M. Ribó, L. Barragán, P. D'Avanzo, D. C. Hannikainen, and E. Kuulkers, Astron. Astrophys. **501**, 1 (2009).
8. J. Chenevez, M. Falanga, S. Brandt, D. Galloway, E. Kuulkers, A. Cumming, H. Schatz, N. Lund, et al., Astron. Telegram **2814**, 1 (2010).
9. D. J. Christian and J. H. Swank, Astrophys. J. Suppl. Ser. **109**, 177 (1997).
10. S. Corbel, P. Kaaret, R. P. Fender, A. K. Tzioumis, J. A. Tomsick, and J. A. Orosz, Astrophys. J. **632**, 504 (2005).
11. N. Degenaar, R. Wijnands, M. T. Reynolds, J. M. Miller, D. Altamirano, J. Kennea, N. Gehrels, D. Haggard, and G. Ponti, Astrophys. J. **792**, 109 (2014).
12. K. Ebisawa, G. Bourban, A. Bodaghee, N. Mowlavi, and T. J.-L. Courvoisier, Astron. Astrophys. **411**, L59 (2003). http://www.isdc.unige.ch/integral/catalog/31/catalog.html
13. D. K. Galloway, M. P. Muno, J. M. Hartman, D. Psaltis, and D. Chakrabarty, Astrophys. J. Suppl. Ser. **179**, 360 (2008).
14. M. Gilfanov, Mon. Not. R. Astron. Soc. **349**, 146 (2004).
15. S. A. Grebenev, M. N. Pavlinsky, and R. A. Sunyaev, in *Proceedings of the Conference on Roentgenstrahlung from the Universe, Wuerzburg, Germany,* Ed. by H. U. Zimmermann, J. E. Truemper, and H. Yorke, MPE Report **263**, 141 (1996).
16. S. A. Grebenev, S. V. Molkov, M. G. Revnivtsev, and R. A. Sunyaev, *Proceedings of the 6th INTEGRAL Workshop on the Obscured Universe,* Ed. by S. Grebenev, R. Sunyaev, and C. Winkler, ESA **SP-622**, 373 (2007).
17. S. A. Grebenev, A. A. Lutovinov, S. S. Tsygankov, and I. A. Mereminskiy, Mon. Not. R. Astron. Soc. **428**, 50 (2013).
18. H.-J. Grimm, M. Gilfanov, and R. Sunyaev, Astron. Astrophys. **391**, 923 (2002).
19. J. J. M. in't Zand, T. G. Patterson, A. C. Brinkman, J. Heise, R. Jager, G. K. Skinner, A. P. Willmore, O. Al-Emam, et al., in *Proceedings of the 23rd ESLAB Symposium on Two Topics on X-ray Astronomy,* Ed. by J. Hunt and B. Battrick, ESA **SP-296**, 693 (1989).
20. J. M. in't Zand, R. Cornelisse, and M. Mendez, Astron. Astrophys. **440**, 287 (2005).
21. P. G. Jonker, R. P. Fender, N. C. Hambly, and M. van der Klis, Mon. Not. R. Astron. Soc. **315**, L57 (2000).
22. P. G. Jonker and G. Nelemans, Mon. Not. R. Astron. Soc. **354**, 355 (2004).
23. N. Kawai and M. Suzuki, Astron. Telegram **534**, 1 (2005).
24. D.-W. Kim and G. Fabbiano, Astrophys. J. **611**, 846 (2004).
25. A. K. H. Kong, L. Homer, E. Kuulkers, P. A. Charles, and A. P. Smale, Mon. Not. R. Astron. Soc. **311**, 405 (2000).

26. R. Krivonos, M. Revnivtsev, E. Churazov, S. Sazonov, S. Grebenev, and R. Sunyaev, Astron. Astrophys. **463**, 957 (2007).
27. R. Krivonos, S. Tsygankov, M. Revnivtsev, S. Grebenev, E. Churazov, and R. Sunyaev, Astron. Astrophys. **523**, A61 (2010).
28. R. Krivonos, S. Tsygankov, A. Lutovinov, M. Revnivtsev, E. Churazov, and R. Sunyaev, Astron. Astrophys. **545**, A27 (2012).
29. R. A. Krivonos, S. S. Tsygankov, A. A. Lutovinov, M. G. Revnivtsev, E. M. Churazov, and R. A. Sunyaev, Mon. Not. R. Astron. Soc. submitted (arXiv:1412.1051) (2014).
30. A. G. Kuranov, K. A. Postnov, and M. G. Revnivtsev, Astron. Lett. **40**, 29 (2014).
31. E. Kuulkers, P. R. den Hartog, J. J. M. in't Zand, F. W. M. Verbunt, W. E. Harris, and M. Cocchi, Astron. Astrophys. **399**, 663 (2003).
32. E. Kuulkers, C. Kouveliotou, T. Belloni, M. Cadolle Bel, J. Chenevez, M. Diaz Trigo, J. Homan, A. Ibarra, et al., Astron. Astrophys. **552**, A32 (2013).
33. F. Lebrun, J. P. Leray, P. Lavocat, J. Crétolle, M. Arqués, C. Blondel, C. Bonnin, A. Bouére, et al., Astron. Astrophys. **411**, L141 (2003).
34. X.-H. Li, F.-J. Lu, and Z. Li, Astrophys. J. **682**, 1166 (2008).
35. D. Lin, D. Altamirano, J. Homan, R. A. Remillard, R. Wijnands, and T. Belloni, Astrophys. J. **699**, L60 (2009).
36. M. Linares, D. Altamirano, A. Watts, T. Strohmayer, D. Chakrabarty, A. Patruno, M. van der Klis, R. Wijnands, et al., Astron. Telegram **3568**, 1 (2011).
37. N. Lund, C. Budtz-Jórgensen, N. J. Westergaard, S. Brandt, I. L. Rasmussen, A. Hornstrup, C. A. Oxborrow, J. Chenevez, et al., Astron. Astrophys. **411**, L231 (2003).
38. A. Lutovinov, M. Revnivtsev, M. Gilfanov, P. Shtykovskiy, S. Molkov, and R. Sunyaev, Astron. Astrophys. **444**, 821 (2005a).
39. A. Lutovinov, M. Revnivtsev, S. Molkov, and R. Sunyaev, Astron. Astrophys. **430**, 997 (2005b).
40. K. O. Mason and F. A. Cordova, Astrophys. J. **262**, 253 (1982).
41. I. A. Mereminsky and S. A. Grebenev, Mon. Not. R. Astron. Soc. (2015, in preparation).
42. S. Migliari, T. Di Salvo, T. Belloni, M. van der Klis, R. P. Fender, S. Campana, C. Kouveliotou, M. Mendez, and W. H. G. Lewin, Mon. Not. R. Astron. Soc. **342**, 909 (2003).
43. S. V. Molkov, A. M. Cherepashchuk, A. A. Lutovinov, M. G. Revnivtsev, K. A. Postnov, and R. A. Syunyaev, Astron. Lett. **30**, 534 (2004).
44. S. Molkov, M. Revnivtsev, A. Lutovinov, and R. Sunyaev, Astron. Astrophys. **434**, 1069 (2005).
45. T. Munoz-Darias, A. de Ugarte Postigo, D. M. Russell, S. Guziy, J. Gorosabel, J. Casares, M. Armas Padilla, P. A. Charles, et al., Mon. Not. R. Astron. Soc. **432**, 1133 (2013).
46. T. Oosterbroek, D. Barret, M. Guainazzi, and E. C. Ford, Astron. Astrophys. **366**, 138 (2001).
47. A. Paizis, K. Ebisawa, H. Takahashi, T. Dotani, T. Kohmura, M. Kokubun, J. Rodriguez, Y. Ueda, et al., Publ. Astron. Soc. Jpn. **61**, S107 (2009).
48. A. N. Parmar, T. Oosterbroek, L. Sidoli, L. Stella, and F. Frontera, Astron. Astrophys. **380**, 490 (2001).
49. M. N. Pavlinsky, S. A. Grebenev, and R. A. Sunyaev, Astrophys. J. **425**, 110 (1994).
50. D. Porquet, J. Rodriguez, S. Corbel, P. Goldoni, R. S. Warwick, A. Goldwurm, and A. Decourchelle, Astron. Astrophys. **406**, 299 (2003).
51. K. A. Postnov and A. G. Kuranov, Astron. Lett. **31**, 7 (2005).
52. M. Revnivtsev, S. Sazonov, K. Jahoda, and M. Gilfanov, Astron. Astrophys. **418**, 927 (2004a).
53. M. G. Revnivtsev, R. A. Syunyaev, D. A. Varshalovich, V. V. Zheleznyakov, A. M. Cherepashchuk, A. A. Lutovinov, E. M. Churazov, S. A. Grebenev, and M. R. Gil'fanov, Astron. Lett. **30**, 382 (2004b).
54. M. Revnivtsev, A. Lutovinov, E. Churazov, S. Sazonov, M. Gilfanov, S. Grebenev, and R. Sunyaev, Astron. Astrophys. **491**, 209 (2008).
55. M. Revnivtsev, K. Postnov, A. Kuranov, and H. Ritter, Astron. Astrophys. **526**, A94 (2011).
56. J. Rodriguez, S. Corbel, I. Caballero, J. A. Tomsick, T. Tzioumis, A. Paizis, M. Cadolle Bel, and E. Kuulkers, Astron. Astrophys. **533**, L4 (2011).
57. M. Sakano, K. Koyama, H. Murakami, Y. Maeda, and S. Yamauchi, Astrophys. J. Suppl. Ser. **138**, 19 (2002).
58. G. Sala and J. Greiner, Astron. Telegram, No. 791 (2006).
59. C. Sanchez-Fernandez, in *Astrostatistics and Data Mining,* Springer Series in Astrostatistics, Ed. by L. M. Sarro, L. Eyer, W. O'Mullane, and J. De Ridder (Springer, New York, 2012), Vol. 2, p. 233.
60. N. Shaposhnikov, C. Markwardt, J. Swank, and H. Krimm, Astrophys. J. **723**, 1817 (2010).
61. G. K. Skinner, A. P. Willmore, C. J. Eyles, D. Bertram, and M. J. Church, Nature **330**, 544 (1987).
62. M. Sugizaki, K. Mitsuda, H. Kaneda, K. Matsuzaki, S. Yamauchi, and K. Koyama, Astrophys. J. Suppl. Ser. **134**, 77 (2001).
63. R. Syunyaev, K. Borozdin, M. Gil'fanov, V. Efremov, A. Kaniovskii, E. Churazov, D. K. Skinner, O. Al-Emam, et al., Sov. Astron. Lett. **17**, 54 (1991a).
64. R. Syunyaev, M. Pavlinskii, M. Gil'fanov, E. Churazov, S. Grebenev, M. Markevich, I. Dekhanov, I. Yamburenko, and G. Babalyan, Sov. Astron. Lett. **17**, 42 (1991b).
65. M. A. P. Torres, D. Steeghs, M. R. Garcia, J. E. McClintock, P. G. Jonker, D. Kaplan, J. Casares, R. Greimel, and T. Augusteijn, Astron. Telegram **784**, 1 (2006).
66. P. Ubertini, F. Lebrun, G. di Cocco, A. Bazzano, A. J. Bird, K. Broenstad, A. Goldwurm, G. la Rosa, et al., Astron. Astrophys. **411**, L131 (2003).
67. W. Voges, B. Aschenbach, Th. Boller, H. Bräuninger, U. Briel, W. Burkert, K. Dennerl, J. Englhauser, et al., Astron. Astrophys. **349**, 389 (1999).

68. S. Wachter and B. Margon, Astron. J. **112**, 2684 (1996).
69. R. S. Warwick, R. D. Saxton, and A. M. Read, Astron. Astrophys. **548**, 99 (2012).
70. N. Werner, J. J. M. in't Zand, L. Natalucci, C. B. Markwardt, R. Cornelisse, A. Bazzano, M. Cocchi, J. Heise, and P. Ubertini, Astron. Astrophys. **416**, 311 (2004).
71. N. J. Westergaard, in *Proceedings of the Conference on the Extreme Sky: Sampling the Universe above 10 keV, Otranto/Lecce, Italy, October 13–17, 2009,* Ed. by P. Ubertini, PoS **96**, 20 (2009).
72. N. E. White and J. van Paradijs, Astrophys. J. **473**, L25 (1996).
73. C. Winkler, T. J.-L. Courvoisier, G. di Cocco, N. Gehrels, A. Gimenez, S. Grebenev, W. Hermsen, J. M. Mas-Hesse, et al., Astron. Astrophys. **411**, L1 (2003).
74. K. S. Wood, J. F. Meekins, D. J. Yentis, H. W. Smathers, D. P. McNutt, R. D. Bleach, E. T. Byram, T. A. Chubb, and H. Friedman, Astrophys. J. Suppl. Ser. **56**, 507 (1984).

Translated by V. Astakhov